Binding Energy Curves from Nonempirical Density Functionals. I. Covalent Bonds in Closed-Shell and Radical Molecules

Adrienn Ruzsinszky and John P. Perdew

Department of Physics and Quantum Theory Group, Tulane University, New Orleans, Louisiana 70118

Gábor I. Csonka*

Department of Inorganic Chemistry, Budapest University of Technology and Economics, H-1521 Budapest, Hungary

Received: June 24, 2005; In Final Form: October 2, 2005

Binding or potential energy curves have been calculated for the ground-state diatomics H_2^+, He_2^+, LiH^+, H_2, N_2, and C_2, for the transition state H_3, and for the triplet first excited state of H_2 using the nonempirical density functionals from the first three rungs of a ladder of approximations: the local spin density (LSD) approximation, the Perdew−Burke−Ernzerhof (PBE) generalized gradient approximation (GGA), and the Tao−Perdew−Staroverov−Scuseria (TPSS) meta GGA. Good binding energy curves in agreement with coupled cluster or configuration interaction calculations are found from the PBE GGA and especially from the TPSS meta GGA. Expected exceptions are the symmetric radicals H_2^+ and He_2^+, where the functionals suffer from self-interaction error, and the exotically bonded C_2. Although the energy barrier for the reaction $H_2 + H \rightarrow H + H_2$ is better in PBE than in TPSS, the transition state H_3 is a more properly positioned and curved saddle point of the energy surface in TPSS. The triplet first excited state of H_2 obeys the Aufbau principle and thus is one of the exceptional excited states that are computable in principle from the ground-state functional. The PBE GGA and TPSS meta GGA are useful not only for chemical applications but also for the construction of higher-rung nonempirical functionals that can further improve the binding energy curves.

1. Introduction and Conclusions

Kohn−Sham density functional theory[1,2] is now the citation leader in both physics[3] and chemistry[4] because it predicts usefully accurate total energies, electron densities, and nuclear frameworks at the computational cost of a self-consistent noninteracting electron problem. For the ground state of nonrelativistic electrons and massive nuclei, these predictions would be exact if the exact spin density functional for the exchange correlation energy $E_{xc}[n_\uparrow, n_\downarrow]$ were known.

The earliest and simplest approximation[1] to $E_{xc}[n_\uparrow, n_\downarrow]$ was the local spin density (LSD) approximation, parametrized, for example, as SVWN5[5] or PWL:[6]

$$E_{xc}^{LSD} = \int d^3r\, n\epsilon_{xc}^{unif}(n_\uparrow, n_\downarrow) \quad (1)$$

where $n_\uparrow(\vec{r})$ and $n_\downarrow(\vec{r})$ are the electron spin densities at position $\vec{r}$, constructed from the occupied Kohn−Sham orbitals:

$$n_\sigma(\vec{r}) = \sum_\alpha^{occup} |\psi_{\alpha\sigma}(\vec{r})|^2 \quad (2)$$

This nonempirical approximation, which becomes exact in the limit of uniform density, is still widely used in solid-state physics.

Considerable improvement in accuracy, especially for molecules, is achieved through the inhomogeneity correction of the generalized gradient approximation[7] (GGA):

$$E_{xc}^{GGA} = \int d^3r\, n\epsilon_{xc}^{unif}(n_\uparrow, n_\downarrow, \nabla n_\uparrow, \nabla n_\downarrow) \quad (3)$$

Still further improvement is achieved by the meta GGA[8]

$$E_{xc}^{GGA} = \int d^3r\, n\epsilon_{xc}^{unif}(n_\uparrow, n_\downarrow, \nabla n_\uparrow, \nabla n_\downarrow, \tau_\uparrow, \tau_\downarrow) \quad (4)$$

where

$$\tau_\sigma(\vec{r}) = \frac{1}{2}\sum_\alpha^{occup} |\nabla\psi_{\alpha\sigma}(\vec{r})|^2 \quad (5)$$

is the noninteracting kinetic energy density or by the hybrid functionals[9] that mix a fraction of exact exchange with GGA or meta GGA exchange.

The functionals can be constructed either empirically by fitting to selected properties of atoms and molecules or nonempirically through the satisfaction of known exact constraints on $E_{xc}[n_\uparrow, n_\downarrow]$. Empirical GGAs[10,11] and hybrids[12,13] are popular in chemistry and have been widely used. There are, however, several advantages[14] to nonempirical functionals: (1) They are as universal as the constraints they respect, working accurately for solid metals and metal surfaces as well as for molecules, whereas the empirical functionals typically do not.[15] (2) They test and deepen the understanding of exchange and correlation. (3) Each rung of the nonempirical ladder of functionals satisfies the exact constraints appropriate to its own set of local ingredients ($n_\uparrow(\vec{r})$, $n_\downarrow(\vec{r})$, ...), whereas the empirical functionals typically satisfy only a few exact constraints. (4) Each rung of the nonempirical ladder builds upon and incorporates the lower rungs. Thus, the Perdew−Burke−Ernzerhof

* Author to whom correspondance should be addressed. E-mail: csonka@web.inc.bme.hu.

10.1021/jp0534479 CCC: $30.25 © 2005 American Chemical Society
Published on Web 11/10/2005

(PBE) GGA[7] on the second rung of the ladder incorporates the LSD of the first rung. Similarly, the new Tao−Perdew−Staroverov−Scuseria (TPSS) meta GGA[8] on the third rung incorporates PBE and may itself be incorporated into higher rungs of the nonempirical ladder.

Although TPSS meta GGA tends to produce more accurate total energies,[16] bond lengths, and vibrational frequencies[17] than PBE GGA, the most striking practical improvements brought about by TPSS are in the atomization or dissociation energies of molecules[17,18] (where TPSS is in some way competitive with the popular empirical functional B3LYP[10−13]) and in the surface energies of metals.[19]

Extensive tests of the nonempirical functionals are needed not only to calibrate them for users but also to determine whether they are robust enough to serve as foundations for future nonempirical functionals on higher rungs. For a given property of a given kind of system, accuracy should increase or at least not decrease up the ladder. A previous meta GGA, the PKZB,[20] was found[21] to fail for the description of hydrogen bonds and had to be replaced by TPSS.[8]

There are now many confirming tests[7,16−19,22−24] of PBE GGA and TPSS meta GGA, but there have been few if any such tests for molecular binding energy curves. For convenience, we shall define the binding or potential energy curve as the total nonrelativistic fixed-nucleus energy E as a function of bond length R; here, we shall not subtract the $R \rightarrow \infty$ limit as is commonly done. Note that this curve defines a potential energy for the nuclear motion in the adiabatic approximation. Calculations of bond length, dissociation energy, and vibrational frequency test the quality of the energy at and near the equilibrium geometry but do not necessarily test its quality under finite expansions and compressions of the bond lengths (as demonstrated by several examples below). We provide such tests here for covalent bonds in closed-shell and radical molecules. Besides the nonempirical functionals LSD, PBE GGA, and TPSS meta GGA, we have made some tests of their one-parameter hybrids PBEh[9] (25% exact exchange) and TPSSh[17] (10% exact exchange) and of the nonempirical Hartree−Fock (HF) or exact-exchange-only method. Because LSD and HF typically display severe over- and underbinding, respectively, we will focus mainly on the more realistic PBE GGA and TPSS meta GGA. A future study will address the van der Waals bonds of the rare-gas and alkaline-earth diatomics.

The main conclusions of the present work may be summarized as follows:

(a) The binding energy curves of the nonempirical PBE GGA and TPSS meta GGA are qualitatively similar to one another and to those of empirical GGAs and hybrids. These curves are qualitatively correct, except for the symmetric radicals H_2^+ and He_2^+ under expansion.[25−30] These symmetric radicals dissociate to fractionally charged fragments (e.g., $H^{+1/2}$ and $H^{+1/2}$) for which LSD, GGA, meta GGA, and hybrid all make substantial self-interaction errors signaled by a spurious maximum in the binding energy curve. But the unsymmetric radical LiH^+, which dissociates to Li^+ and H, is properly described. (Approximate functionals do not always dissociate molecules to correctly charged atoms, but the spin density functional description of LiH^+ is nonproblematic. We hope to search for problematic cases in future work.)

(b) For these density functionals, as for single-reference wave function methods such as the coupled cluster method, spin symmetry breaking[32−34] is often needed to make a realistic binding energy curve, especially at expanded bond lengths. The spin symmetry breaking in stretched H_2 and N_2 is rather similar in PBE GGA and TPSS meta GGA.

(c) For C_2, where the singlet spin symmetry is broken even at the equilibrium bond length,[35,36] the detailed shape of the true ground-state binding energy curve that arises from many low-lying excited states[36,37] is not well described by GGA or meta GGA.

(d) The equilibrium bond length and equilibrium total energy of a molecule tend to be described very well by the TPSS meta GGA, in some cases, better than by simple implementations of the coupled cluster or full configuration interaction methods.

(e) The energy barrier for the reaction $H_2 + H \rightarrow H + H_2$ is too low in PBE GGA and even lower in TPSS meta GGA, although for a large set of molecules, the errors in the energy barriers are about the same for both functionals.[38,39] Nevertheless, the energy surface near the transition state H_3 is a properly positioned and properly curved saddle point in TPSS meta GGA, whereas it is improperly positioned and improperly curved in PBE GGA (as in some other GGAs[40]), and it is a global minimum in LSD. The good TPSS description of the H_3 energy surface near its saddle point is consistent with the good TPSS description of molecular vibrational frequencies.[17]

(f) The binding energy curve of the essentially repulsive triplet (fully spin-polarized) first excited state[41] of H_2 is reproduced accurately by PBE GGA and especially by TPSS meta GGA. Even the very weak van der Waals minimum is found. Because its orbital energies obey the Aufbau principle, this is one of the exceptional excited states that are computable from the ground-state density functional according to the spin density functional generalization of ref 42.

On the basis of these and other studies, we conclude that PBE GGA and TPSS meta GGA are not only useful functionals for chemical applications but also are firm and secure rungs on which to construct higher-rung nonempirical functionals. The fourth (and still incomplete) rung is the hyper GGA, which should employ full (100%) exact exchange and a compatible, fully nonlocal, self-interaction-free correlation functional. In the hyper GGA, the binding curve of H_2^+ should be exact, and that of He_2^+ should be improved. The energy barriers of H_3 and other transition states should also be raised, but the binding curve for C_2 might remain a challenge.

2. Methods of Calculation

We performed most of our calculations with triple-ζ-quality basis sets, which have proved reliable for density functional computations, using the Gaussian 03 program package[43] with the Suse Linux 9.0 operating system. Basis set effects were also studied for several compounds from the simplest 6-31G(d) basis set up to the largest aug-cc-pVQZ. These basis sets are built into Gaussian 03. We observed some SCF convergence problems with the Gaussian 03 implementation of the TPSS method for H_3 with the usual DIIS SCF convergence acceleration procedure, so instead of that we used CDIIS, NoDIIS, and SCF=QC procedures as necessary (vide infra).

In many cases, we performed quantum chemical (e.g., CCSD-(T), that is, nearly equivalent to full CI for two- and three-electron systems) calculations for comparison with those from density functional theory. The quantum chemical methods generally require larger basis sets than the density functional methods do. We do not claim that our quantum chemical total energies are converged with respect to the basis set limit, but we suspect that their binding energy curves are otherwise reasonably shaped in most cases; that is, that they are converged around equilibrium apart from an overall vertical shift of the

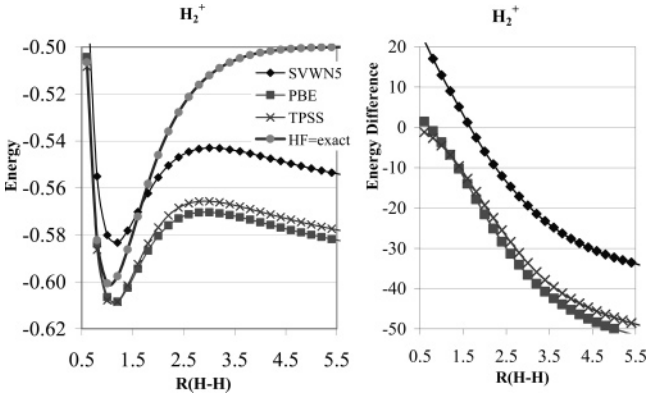

Figure 1. H_2^+ ground-state ($^2\Sigma_g$) binding energy curves (hartree) calculated with HF, SVWN5, PBE, and TPSS methods using the 6-311G(d,p) basis set. The panel on the right shows the corresponding energy differences (in kcal/mol) of the SVWN5, PBE, and TPSS curves from the essentially exact Hartree−Fock curve. The H−H distance is in Å. (1 hartree = 627.5 kcal/mol; 1 bohr = 0.5292 Å.)

total energy. (For example, standard basis functions for second-row atoms such as Li typically do not include the core polarization functions needed to converge the correlation energy of the 1s core in a CI or coupled cluster calculation). In each Figure, we also report the exact nonrelativistic energy in the dissociation limit.[44,45]

3. Radical Diatomic Cations (H_2^+, He_2^+, LiH^+) and the Self-Interaction Error

Molecules with an odd number of electrons can be problematic for approximate density functionals.[25−30] The simplest and most dramatic example is the one-electron molecule H_2^+ (Figure 1). In the ground state, the electron spends half its time on each nuclear center. At large internuclear separation R, the lowest-energy self-consistent solution predicted by the semilocal spin density functional approximations is $H^{+0.5}\cdots H^{+0.5}$ ($D_{\infty h}$ symmetry). Another broken-symmetry ($C_{\infty h}$) solution of higher energy and less stability is of course $H^{+1}\cdots H^0$, which leads to the correct dissociation limit (discussion of covalent and ionic dissociation limits for H_2^+ in ref 29). The fractional electron number on each site leads to a large, negative self-interaction error[29,31,46,47] in the total energy at large R and to a spurious maximum in the binding energy curve, as shown in Figure 1 in agreement with ref 29. The distance dependence of the self-interaction error for dissociating H_2^+ is shown in Figure 2a of ref 29, and an approximate formula for the distance dependence of the self-interaction error is also given in ref 29 (cf. eq 8). According to ref 29 the self-interaction error is dominant above 5 Å R(H−H).

For the one-electron molecule H_2^+, the self-interaction-free HF method is exact (apart from small basis set errors), and it shows no spurious maximum in Figure 1. We note that an admixture of 10 to 25% of exact exchange in a hybrid functional can produce only a minor improvement in the large-R behavior of the PBE or TPSS binding curves for H_2^+, as we will show for He_2^+. Around the minimum, however, the PBE and TPSS functionals are not so badly behaved.

The three-electron molecule He_2^+ (Figure 2) is another symmetric radical, very much like H_2^+. For this molecule our CCSD(T) binding energy curve has the right qualitative shape, whereas again the density functional methods show a spurious maximum.

LiH^+ (Figure 3) is another three-electron molecule but an asymmetric one for which the density functionals dissociate to

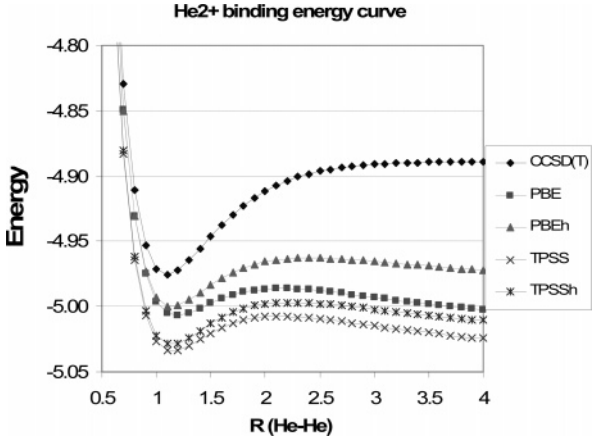

Figure 2. Symmetric He_2^+ ground-state binding energy curve (hartree) calculated with CCSD(T), PBE, PBEh, TPSS, and TPSSh methods using the 6-311G(d,p) basis set. Interatomic distances are in Å. The exact nonrelativistic dissociation limit ($R \rightarrow \infty$)[44,45] has the energy −4.904 hartrees.

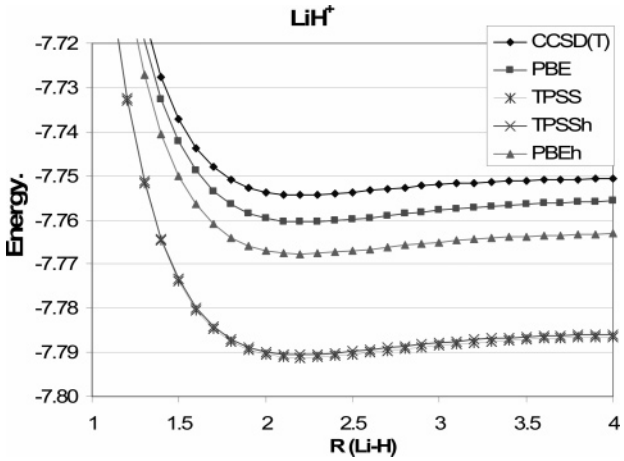

Figure 3. LiH^+ potential energy curves (hartree) calculated with CCSD(T), PBE, PBEh, TPSS, and TPSSh methods using the 6-311G-(d,p) basis set. Interatomic distances are in Å. The exact nonrelativistic dissociation limit ($Li^+\cdots H$ with $R \rightarrow \infty$)[44,45] has the energy −7.780 hartree. (CCSD(T) total energy misses 67% of the correlation energy of the Li^+ 1s core because of the basis set limitation, but this does not affect the shape of the curve.)

$Li^+\cdots H$ separated fragments of integer charge for which the self-interaction errors are small. Figure 3 shows that all of the binding energy curves have the same correct shape as the CCSD-(T) curve. The total energy is actually most correct in TPSS, which converges much faster with respect to the basis set than CCSD(T) does.

4. Closed-Shell Diatomics (H_2, N_2) and Spin Symmetry Breaking

It is well known that when the many-electron Hamiltonian commutes with mutually commuting total-spin operators the eigenstates of the former can be chosen to be eigenstates of the latter operators. The molecules of H_2 (Figure 4) and N_2 (Figure 5) are closed-shell systems in which the true ground states for all internuclear separations R are spin singlets with zero net spin density. For H_2, the spin-restricted CCSD(T)/6-311G(d,p) model (equivalent to full CI for this two-electron system) produces a qualitatively correct binding curve, whereas for N_2, the restricted CCSD(T)/6-311G(d,p) model calculation displays a spurious maximum at large R. This spurious maximum is a failure of single reference quantum chemistry as discussed in

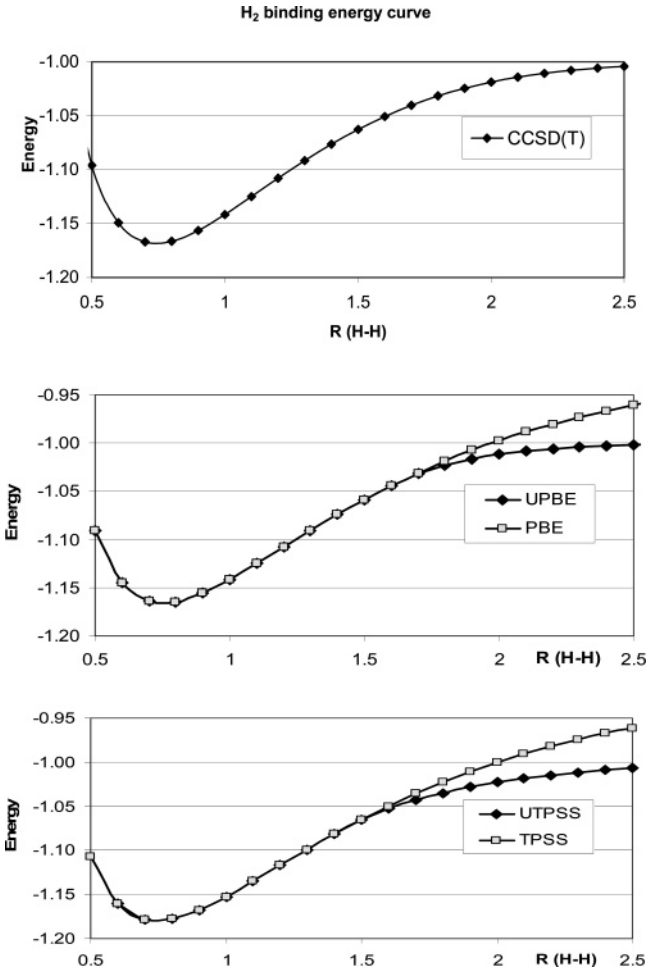

Figure 4. Restricted and unrestricted CCSD(T), PBE, and TPSS/6-311G(d,p) potential energy curves of the dissociating H_2 molecule, showing spin symmetry breaking. The exact nonrelativistic dissociation limit ($R \rightarrow \infty$) has the energy −1.000 hartree. The H−H distance is in Å.

ref 48 and confirmed here with the larger basis set (of triple- instead of double-ζ quality). It disappears in the spin-unrestricted UCCSD(T)/6-311G(d,p) model, which starts from a symmetry-broken HF wave function. For further discussion see refs 49 and 50.

For these molecules, the approximate density functionals produce no spurious spin density near equilibrium, but spurious spin density appears when R increases through the Coulson−Fischer point where the spin-unrestricted (U) solution (using guess=mix in Gaussian 03) becomes energetically lower than the spin-restricted one. As $R \rightarrow \infty$, the unrestricted solution produces two separate atoms with opposite spin moments. This spin symmetry breaking[32−34] produces a significant improvement in the shape of the binding energy curve for reasons that are well understood.[34] From one point of view, the symmetry breaking just freezes out energetically important spin correlations in the ground state of the dissociating molecule that the functional could not account for in a spin-restricted formalism. For example, consider the singlet ground state of Cr_2 at equilibrium. The average spin density vanishes everywhere, but fluctuations around this average show a strong tendency to have spin up on one atomic site and spin down on the other atomic site, as reflected by the spin symmetry broken spin densities predicted by semilocal spin density approximations.

In H_2, the Coulson−Fischer symmetry breaking points are $R = 1.7$ Å in UPBE and $R = 1.5$ Å in UTPSS using the 6-311G-

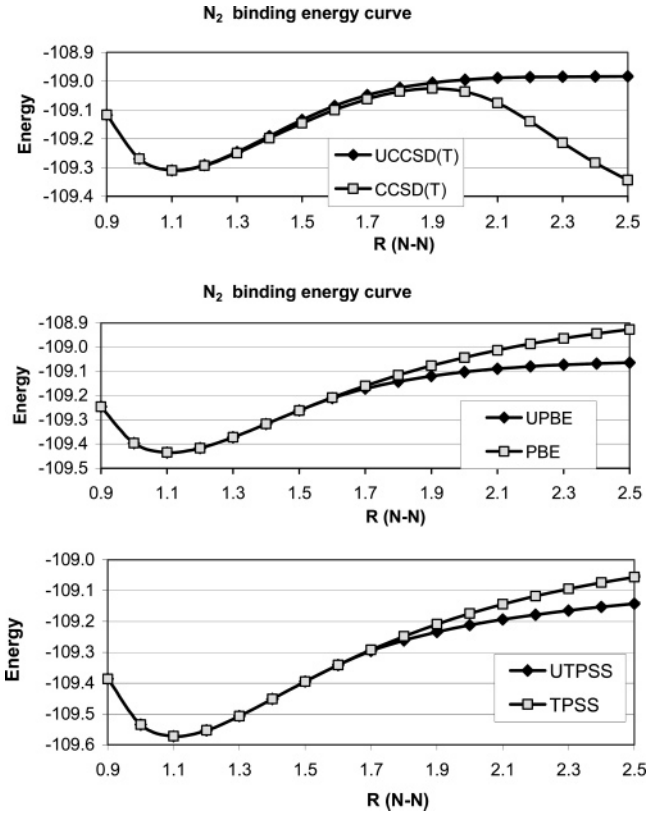

Figure 5. Restricted and unrestricted CCSD(T), PBE, and TPSS/6-311G(d,p) potential energy curves of the dissociating N_2 molecule in its $^1\Sigma_g^+$ ground state, showing the spin symmetry breaking. The exact nonrelativistic dissociation limit ($R \rightarrow \infty$)[44,45] has the energy −109.178 hartrees. The N−N distance is in Å.

(d,p) basis set for both. In N_2 they are $R = 1.6$ Å in UPBE and $R = 1.7$ Å in UTPSS. These results are similar to the UBLYP result for N_2 ($R = 1.5$ Å) from Polo et al.[51]

Density functional calculations are normally performed in a spin-unrestricted (U) mode, so the symbol U is normally suppressed. In this and the following section, however, we stress the spin symmetry breaking by displaying the symbol U.

5. Exotically Bonded C_2 Molecule

C_2 is a molecule with several low-lying spin states, including a singlet ground state and several singlet excited states. The spin symmetry breaks even at the equilibrium bond length in both Hartree−Fock[37] and spin density functional theories.[35,36]

The X $^1\Sigma_g^+$ ground electronic state exhibits very unusual bonding, having two π bonds but no σ bond. The deficiencies in RHF or UHF wave functions are so severe that, in general, they cannot be adequately corrected by the addition of electron correlation via single-reference perturbation theory or coupled cluster theory at larger atomic distances. Multireference methods, for example, a complete active space self-consistent field with second-order perturbation theory corrections (CASPT2[52]), can accurately model such problems. However, they are computationally more expensive and not widely available in program packages.

Recent full CI/6-31G(d) results[37] show that some of the qualitative features of the full CI binding energy curves are accurately captured using this modest basis set. The B $^1\Delta_g^+$ excited state crosses below the X $^1\Sigma_g^+$ ground electronic state around 1.7 Å, and the two states remain very close in energy (with differences of less than 3 kcal/mol) as they approach the same asymptotic dissociation limit of 2 C (^{3}P); they are nearly

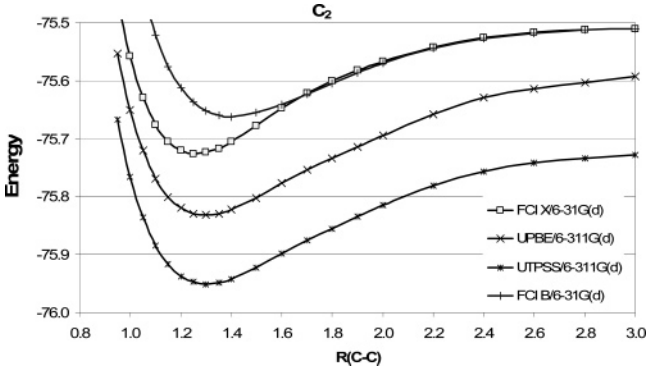

Figure 6. Full CI/6-31G(d) binding energy (hartree) curves (from ref 37) for the X $^1\Sigma_g^+$ and B $^1\Sigma_g^+$ states (noted as X and B, respectively) of dissociating C_2 and the corresponding spin symmetry broken SSB UPBE/6-311G(d) and SSB UTPSS/6-311G(d) curves. The exact nonrelativistic dissociation limit ($R \rightarrow \infty$)[44,45] has the energy −75.690 hartrees. The C−C distance is in Å.

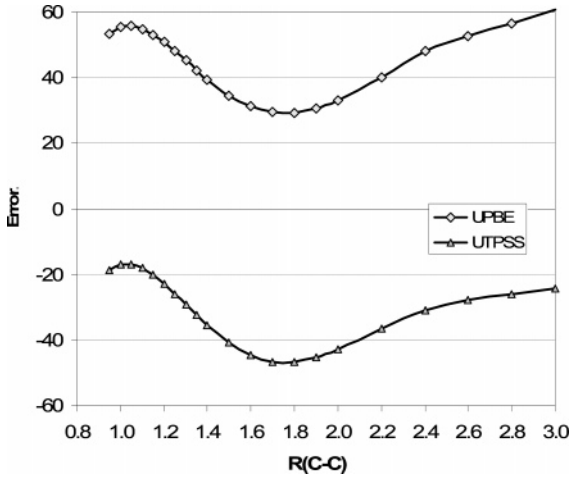

Figure 7. SSB UPBE/6-311G(d) and UTPSS/6-311G(d) errors (SSB density functional energy − reference, kcal/mol) in the binding energy curves for the dissociating ground-state C_2 molecule. The reference is the full CI/6-31G(d) energy taken from ref 37, shifted to recover the exact nonrelativistic dissociation limit from the caption of Figure 6. The C−C distance is in Å. The nonparallelity error around equilibrium is much larger for C_2 than for LiH^+, H_2, N_2, or the triplet excited state of H_2.

degenerate at 2.8−3.0 Å. Above 1.8 Å the characters of the X $^1\Sigma_g^+$ state and a third B′ $^1\Sigma_g^+$ state are reversed because of an avoided crossing.[37] This leads to an unusual shape for the ground-state binding energy curve, which does not look like a typical Morse potential. The approximate single-reference methods have considerable difficulty reproducing this shape. Whereas the restricted methods tend to have the greatest difficulty at large distances, unrestricted methods have more trouble in the intermediate region. Errors for UHF-based methods near equilibrium and the dissociation limit are quite small for SSB UCCSD and UCCSD(T), but they become as large as 31 and 24 kcal/mol, respectively, at intermediate distances.[37] It was observed that even iterative triples in full CCSDT or triples and quadruples in CISDTQ are insufficient to achieve quantitatively reliable results.[37]

Figure 6 shows the full CI/6-31G(d) potential energy curves for the X $^1\Sigma_g^+$ and B $^1\Delta_g^+$ states (noted as X and B, respectively) of dissociating C_2[37] and the corresponding spin symmetry broken (SSB) UPBE and UTPSS curves using the larger 6-311G(d) basis set. We found that the larger basis set does not yield qualitatively different UPBE and UTPSS curves from the smaller one. It was observed earlier by Abrams et al.[37] that the

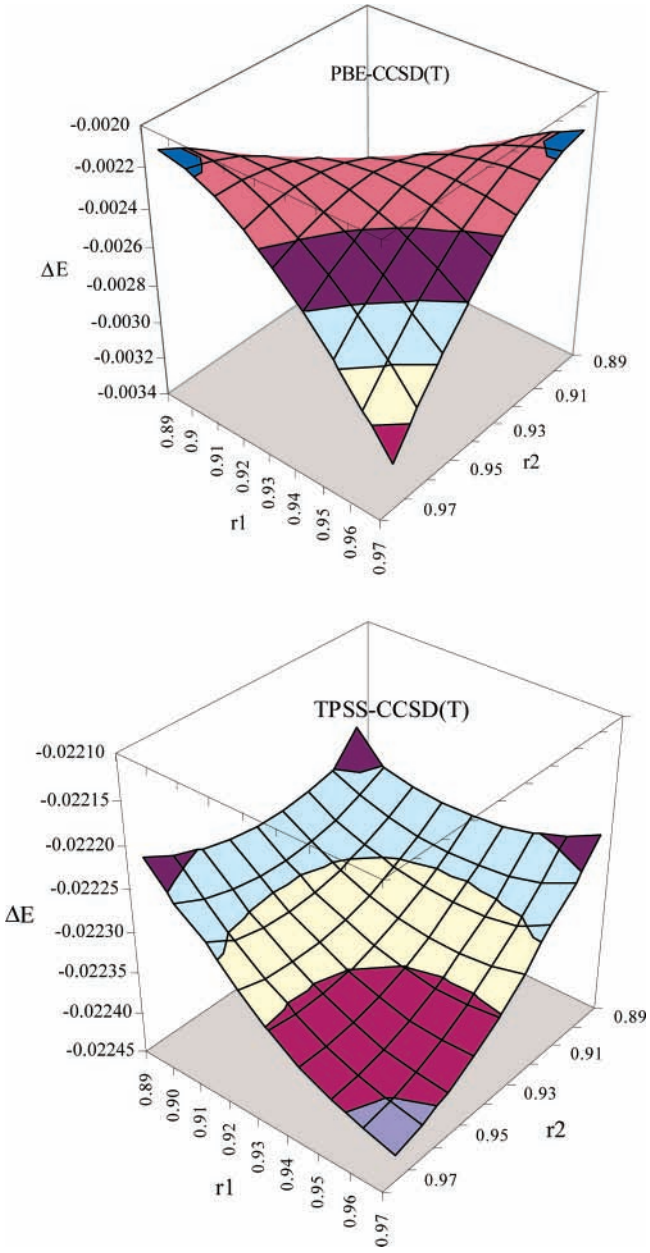

Figure 8. Energy surface differences (hartree) relative to CCSD(T) for the H_3 $C_{\infty v}$ structure. r_1 and r_2 are the two internuclear distances (Å). The 6-311++G(d,3pd) basis set was used for these calculations.

C_2 molecule is unusual in that the SSB UHF binding energy curve is lower than the RHF binding energy curve even at short internuclear distances. We observed that the restricted PBE and TPSS binding energy curves run above the corresponding SSB UPBE and SSB UTPSS curves at short C−C distances (0.95−1.2 Å), as the RHF and SSB UHF curves do. The Coulson−Fischer symmetry breaking point is at 0.95 Å internuclear distance for the PBE curves, independent of the two basis sets used in this study.

A detailed discussion of C_2 at the GGA level of description was presented in ref 35. At the equilibrium bond length (about 1.3 Å), the PW91 GGA places the broken-symmetry singlet state 4.8 kcal/mol above the triplet state, although experimentally[53] the singlet is 2.1 kcal/mol below the triplet state. The PBE GGA and TPSS meta GGA place the broken-symmetry singlet 2.8 and 3.0 kcal/mol above the triplet, respectively, improving somewhat on PW91. The electronic atomization energies D_e from the broken-symmetry singlet at equilibrium

TABLE 1: Hydrogen Atom Total Energies $E(H)$ (hartree), Hydrogen Molecule Total Energies $E(H_2)$ (hartree), Hydrogen Molecule Equilibrium Distances $R(H-H)$ (Å), H_3 Energy $E(H_3)$ (hartree), H_3 Barrier Distances $r_1 = r_2$ (Å), and the Classical Hydrogen Abstraction Energy Barriers (kcal/mol)

method	$E(H)$	$E(H_2)$	$R(H-H)$	$E(H_3)$	$r_1 = r_2$	barrier
CCSD(T)/6-311++G(d,3pd)	−0.49982	−1.17253	0.7420	−1.65652	0.9304	9.93
CCSD(T)/6-311G(d,3pd)	−0.49981	−1.17251	0.7420	−1.65643	0.9306	9.97
CCSD(T)/6-311G(d,2pd)	−0.49981	−1.17231	0.7427	−1.65620	0.9300	9.99
QCISD/6-311G(d,2pd)	−0.49981	−1.17231	0.7426	−1.65579	0.9300	10.25
CCSD(T)/6-311G(d,2p)	−0.49981	−1.17082	0.7420	−1.65393	0.9296	10.48
CCSD(T)/6-311G(d,p)	−0.49981	−1.16834	0.7435	−1.65039	0.9290	11.14
TPSS/6-311++G(d,3pd)	−0.50004	−1.17985	0.7434	−1.67887	0.9318	0.64
TPSS/6-311G(d,3pd)	−0.49987	−1.17983	0.7433	−1.67876	0.9319	0.59
TPSS/6-311G(d,2pd)	−0.49987	−1.17982	0.7435	−1.67860	0.9324	0.68
TPSS/6-311G(d,p)	−0.49987	−1.17955	0.7441	−1.67783	0.9329	1.00
PBE/6-311G(d,2pd)	−0.49962	−1.16615	0.7507	−1.65985	0.9371	3.71
PBEh/6-311G(d,2pd)	−0.50104	−1.16849	0.7455	−1.66047	0.9300	5.68
SWVN5/6-311++G(d,3pd)	−0.47851	−1.13728	0.7660	−1.62024	0.9496	−2.80
SWVN5/6-311G(d,p)	−0.47835	−1.13692	0.7670	−1.61963	0.9503	−2.74
HF/6-311++G(d,3pd)	−0.49982	−1.13307	0.7343	−1.60488	0.9330	17.58
HF/6-311G(d,p)	−0.49981	−1.13249	0.7354	−1.60433	0.9340	17.55
expt[a]	−0.50000	−1.17447	0.7414			9.70

[a] References 56 and 58.

are 151.1 kcal/mol for PW91, 155.6 kcal/mol for PBE, 143.3 kcal/mol for TPSS, and 146.7 kcal/mol experimentally.[54] Despite the good performance of the functionals for atomization energies, the detailed shape of the binding energy curve for C_2 is predicted rather poorly, as discussed in the next paragraph.

Figure 7 shows the deviations of the SSB UPBE and SSB UTPSS binding energy curves from a corrected full CI/6-31G(d) curve[37] for X $^1\Sigma_g^+$ C_2. It can be seen that the SSB UPBE and SSB UTPSS error curves are parallel; the UPBE deviation is typically larger. The largest errors can be observed around $R = 1.8$ Å.

The spin symmetry breaking found here in PBE and TPSS is qualitatively like that of PW91 from ref 35. Near equilibrium, the up and down spin densities are concentrated not on the atoms but on opposite sides of the bond between the atoms. At large R, the up and down spin densities are atom-centered. However, a direct energy scan with Gaussian 03 tends to produce PBE and TPSS self-consistent solutions for C_2 at large R that rise above the energy of two separated carbon atoms. To get the lowest-energy solutions, we started the iteration from a checkpoint file kindly provided by Dr. Viktor Staroverov and available on the website web.inc.bme.hu/csonka/p96.html.

6. H_3 Transition State Radical

The H_3 radical is not a stable system, but it is the transition state for the simplest hydrogen abstraction reaction $H_2 + H \rightarrow H + H_2$. This reaction is of fundamental, practical, and theoretical significance. The practical importance arises from the observation that the rate-limiting step in some combustion reactions is the abstraction of a hydrogen atom from saturated hydrocarbons. Because there are three nuclei instead of two and the nuclei lie on a line, the H_3 binding energy curve is replaced by an energy surface in a 2D space.

We carried out an energy scan for both H−H distances r_1 and r_2 of the H_3 radical between 0.89 and 0.97 Å with a 0.01 Å step size. We first compared the TPSS and PBE/6-311++G(d,3pd) energy scan results to the corresponding CCSD(T)/6-311++G(d,3pd) energies. The energy differences (DFT-CCSD(T)) are shown in Figure 8. It can be observed that in the given domain around the saddle point the TPSS method follows the CCSD(T) energy surface considerably better than the PBE method does. The TPSS functional not only yields a better surface around the saddle point but also yields an H−H distance (0.931 Å) for the saddle point that agrees with the CCSD(T) saddle point H−H distance (0.931 Å, cf. Table 1). The corresponding PBE result is 0.937 Å. We noted that the current implementation of the TPSS functional has shown SCF convergence problems, so several points of the surface in Figure 8 were obtained by the use of a quadratically′ convergent SCF procedure (SCF=QC). Earlier[40] it was observed that GGA functionals such as BPW91 and BLYP yield a consistently longer (0.934 Å) saddle point H−H distance, as does PBE (0.937 Å), and BP86 yields a qualitatively incorrect minimum instead of a saddle point. The corresponding hybrid functionals yield a qualitatively correct energy surface around the saddle point and H−H saddle point distances around 0.930 Å.[40] Interestingly, the TPSS functional is able to yield a good-quality surface curvature without mixing exact exchange. This feature is also shown in Figure 9, where we present the energies for the symmetric and asymmetric stretching curves. In the symmetric stretching curve, the two r_1 and r_2 H−H distances are equal ($r_1 = r_2$), whereas in the asymmetric stretching curve $r_1 + r_2 = 1.86$ Å. A vibrational frequency calculation can determine if the critical point $r_1 = r_2$ is a saddle point.

We studied several functionals—SVWN5, PBE GGA, and TPSS meta GGA—for the symmetric and asymmetric stretching potential energy curves of H_3. We observed that the SVWN5 functional provides a false energy minimum for the H_3 structure as shown in Figure 9, and its false binding energy is shown in Table 1. The PBE functional cannot provide the right position for the saddle point, and it fails to yield the correct asymmetric stretching curve shown in the Figure. In contrast, TPSS meta GGA is able to provide the correct asymmetric stretching curve. Similar energy curves were calculated with the CCSD(T)/6-311G(d,p) model and are shown in Figure 9. The asymmetric stretching curve of the CCSD(T) method has a maximum at 0.930 Å, and this is found on the TPSS asymmetric stretching curve as well. However, we can see a shallow minimum in the asymmetric stretching curve with PBE starting from 0.930 Å.

An analysis of the results in Table 1 shows that for the H_3 classical barrier height the CCSD(T)/6-311G(d,2pd) result (9.99 kcal/mol) is almost converged to the most expensive CCSD(T)/6-311++G(d,3pd) result (9.93 kcal/mol). High-quality quantum Monte Carlo (QMC) calculations yield 9.613 ± 0.006 kcal/mol for the barrier height,[55] which is very close to the experimental value of 9.7 kcal/mol[56] and only slightly lower

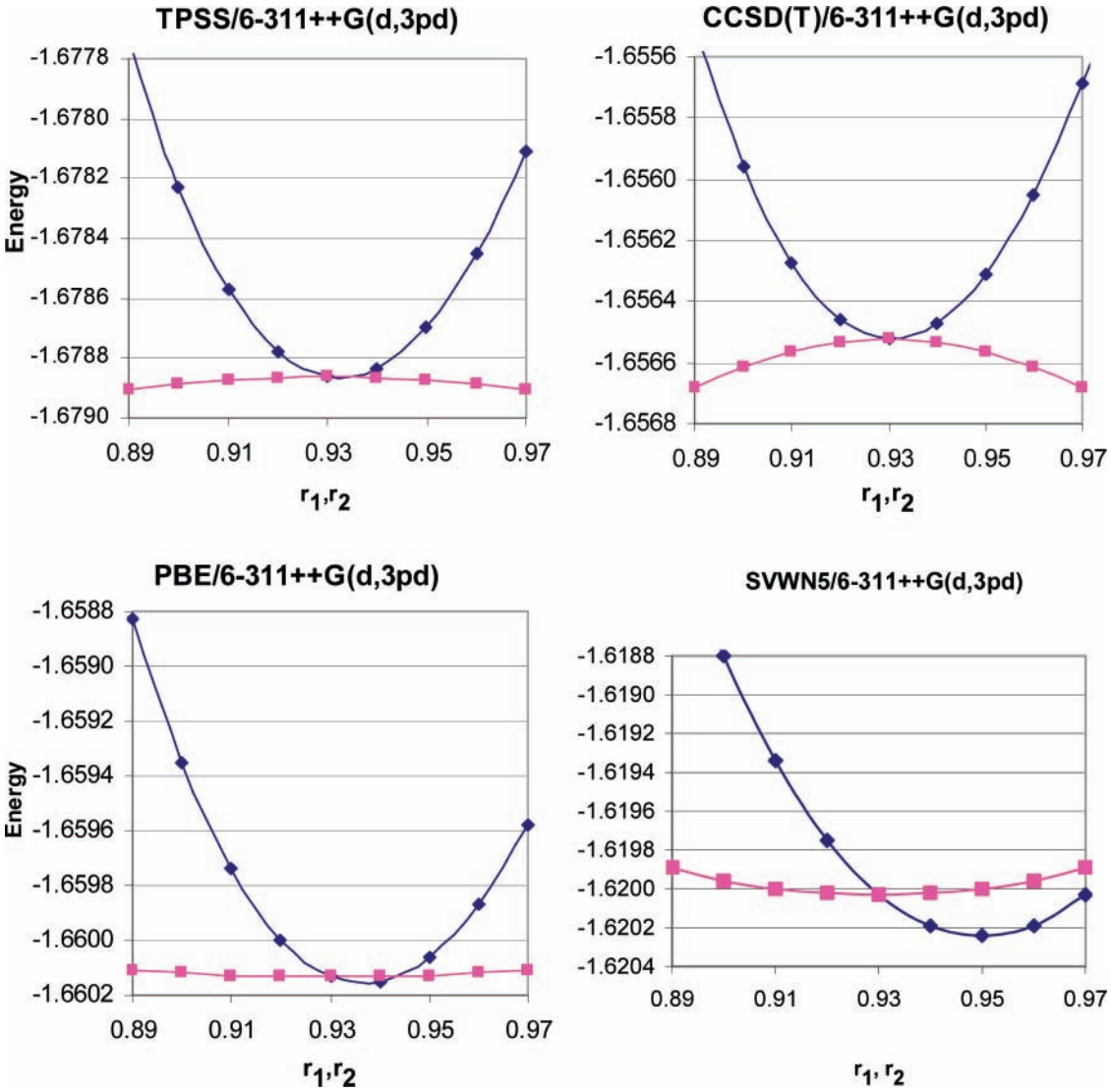

Figure 9. Symmetric (blue, $r_1 = r_2$) and asymmetric (pink, $r_1 + r_2 = 1.86$ Å) stretching energy curves (hartree) for the H_3 $C_{\infty v}$ structure. r_1 and r_2 are the two internuclear distances (Å). Note that the asymmetric stretch is not the path that minimizes E for a given r_1 because r_2 is constrained to be 1.86 Å $- r_1$.

than the CCSD(T)/6-311G(d,2pd) result. However, smaller basis sets lead to a considerably larger barrier height for the CCSD(T) model (up to 11.14 kcal/mol with the CCSD(T)/6-311G(d,p) model, cf. Table 1). The HF, SVWN5, and PBE methods show little basis-set dependence for the barrier height (cf. Table 1). The HF method yields too high a barrier, whereas the SVWN5 method yields a stably bonded H_3 (no barrier). The PBE results show an important improvement compared to the SVWN5 results, but the calculated barrier height remains too low. The hybrid PBE shows an improved barrier height (5.68 kcal/mol). Despite the good curvature and position of the barrier, the TPSS method yields too low a barrier height (less than 1 kcal/mol, cf. Table 1). Mixing the TPSS with 10% exact exchange[17] yields a marginally increased barrier height (by about 0.5 kcal/mol), and even 25% exact exchange mixing adds only 1.3 kcal/mol to the barrier height. As noted earlier,[40] the self-interaction error causes the low barrier. Applying the Perdew−Zunger self-interaction correction[46] increases the barrier height obtained from GGA functionals by about 9−10 kcal/mol.[40]

Finally, we discuss in detail why the TPSS energy barrier for the reaction $H_2 + H \rightarrow H + H_2$ is too low. Table 1 shows that in TPSS the energies of H and H_2 are highly accurate, whereas the energy of the H_3 transition state is too negative. TPSS has an exchange-correlation hole[57] that is localized around its electron like the exact hole in H and H_2. But in H_3 there is just one $\downarrow$ electron whose orbital and exchange hole are spread uniformly over three fairly distant nuclear centers, so the exact exchange-correlation hole is partially delocalized, resulting in a higher energy than that of the TPSS hole. Fixing the TPSS barrier probably requires using exact exchange as in a hyper GGA.

7. Triplet First Excited State of H_2

Normally, Kohn−Sham calculations with the ground-state density functional predict only the ground state; the excited-state solutions are not meaningful in principle. However, an exception occurs when the excited-state solution satisfies the Aufbau principle with all occupied orbital energies below all unoccupied ones. In the latter case, an excited state is obtained as an extremum of the ground-state functional.[42,59,60] An example is the triplet first excited state of H_2. For this state, it is clear that the Aufbau principle must be satisfied in the limit $R \rightarrow \infty$, where the $1\sigma_{g\uparrow}$ and $1\sigma_{u\uparrow}$ orbitals become degenerate, but we find that the Aufbau principle is satisfied even around the shallow minimum of the binding curve and even at $R = 2.0$ Å.

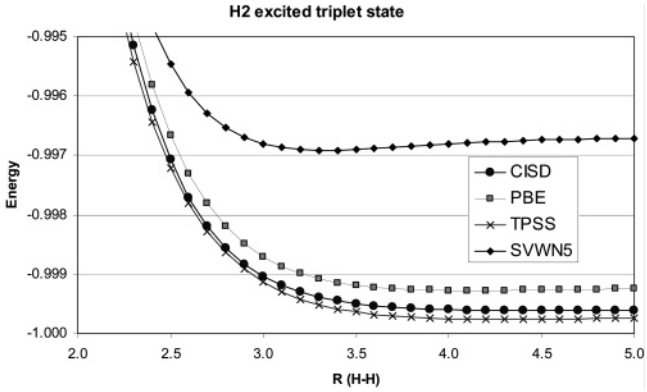

Figure 10. Full CI, SVWN5, PBE, and TPSS/6-311G(d,p) energy curves for the H_2 b $^3\Sigma_u^+$ triplet first excited state. Energy in hartree and R(H−H) in Å. SVWN5 energy curve was shifted by −0.04 hartree. The exact nonrelativistic dissociation limit is −1.000 hartree.

Both the X $^1\Sigma_g^+$ and the b $^3\Sigma_u^+$ states of the H_2 molecule dissociate to the limit of H(1s) + H(1s). The full CI results show that ground state X $^1\Sigma_g^+$ arises from the configuration $|1\sigma_g^2\rangle$, whereas the b $^3\Sigma_u^+$ state results from the configuration $|1\sigma_g 1\sigma_u\rangle$. The b $^3\Sigma_u^+$ triplet state, according to Kolos and Wolniewicz,[41] is predominantly repulsive except for a shallow vdW minimum around R(H−H) ≈ 4.1 Å with an estimated binding energy of about 4 cm^{-1}. Other calculations[61,62] confirm the existence of a vdW minimum.

An analysis of the binding energy curves shown in Figure 10 shows that the SVWN5 curve is quantitatively and qualitatively incorrect, showing a relatively steep minimum at R(H−H) ≈ 3.3 Å. The deviation between the full CI and the SVWN5 curves is large; at R(H−H) = 5 Å, the full CI curve is well below the SVWN5 curve (by −0.04291 hartree); consequently, we have shifted the SVWN5 curve shown in Figure 10 by −0.04 hartree. The PBE curve has improved considerably compared to the SVWN5 curve, showing a very shallow minimum at R(H−H) ≈ 4.1 Å and running very close to the full CI curve and slightly above it. The TPSS curve shows a further improvement, running closer to the full CI curve and showing an even more shallow minimum at R(H−H) ≈ 4.4 Å. Our tests show that these results are stable against the increase of the basis set (vide infra). (Note that the TPSS binding curve of triplet H_2 has been studied independently by V. N. Staroverov and E. R. Davidson. Private communication.) The full CI curve is used only as a qualitative reference because it was calculated with a relatively small basis set; however, it seems to be sufficient to show the improvements along the density functional ladder. A comparison of SVWN5 and PBE curves to those calculated with the aug-cc-pVQZ basis set shows that the aug-cc-pVQZ curves run parallel to the 6-31G(d,p) curves, preserving the positions of the minima. Figure 11 shows the full CI, SVWN5, PBE, and TPSS relative binding energy curves ($E(R_{H-H}) - 2*E(H)$) calculated with the aug-cc-pVQZ basis set. Although Figure 10 does not reveal the minimum of the full CI/6-311G(d,p) energy at R(H−H) ≈ 4.1 Å, this minimum can be observed in Figure 11. The largest basis-set dependence can be observed for the full CI relative binding energy curve; however, the SVWN5 curve also shows a considerable basis-set dependence. The PBE and the TPSS functionals show considerably less basis-set dependence; for example, the TPSS/6-311G(d,p) curve is parallel to the TPSS/6-311G(d,p)/aug-cc-pVQZ curve in the range of 3−4 Å H−H distance, as shown in Figure 12. At shorter distances the basis-set effects are more important; however, they remain small for the PBE and TPSS functionals. This is a very desirable behavior.

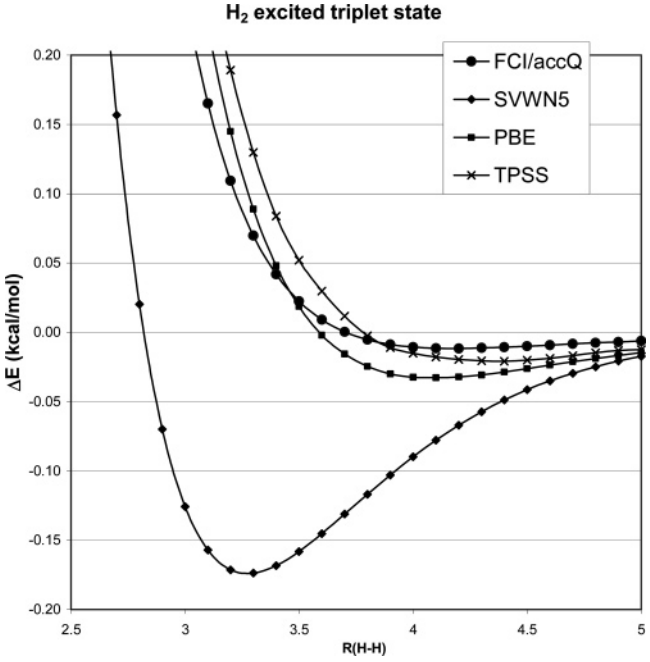

Figure 11. Full CI, SVWN5, PBE, and TPSS/aug-cc-pVQZ relative binding energy [$E(R_{H-H}) - 2*E(H)$] curves for the H_2 b $^3\Sigma_u^+$ triplet first excited state. R(H−H) is in Å. Note the shallow van der Waals minimum for each curve.

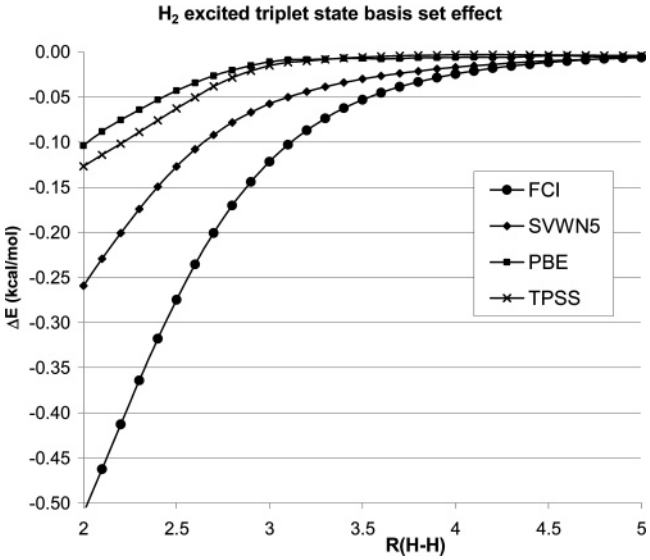

Figure 12. Full CI, SVWN5, PBE, and TPSS basis-set energy differences ($E_{aug-cc-pVQZ} - E_{6-311G(d,p)}$) in the relative binding energy curves for the H_2 b $^3\Sigma_u^+$ triplet first excited state. R(H−H) is in Å.

We might imagine stabilizing the ↑↑ triplet state of H_2 as a ground state by applying a strong, uniform magnetic field that couples only to the spin. Then its binding energy curve would be expected to resemble that of two closed-shell atoms, for example, He_2. In this sense, our study of triplet H_2 is a prelude to our coming study of binding curves for the rare-gas dimers.

Acknowledgment. A.R. acknowledges fellowship support from the Pro Progressio Foundation and OTKA under grant PD050014. J.P.P. acknowledges the support of the U.S. National Science Foundation under grants DMR-01-35678 and DMR-05-01588, and G.I.C. acknowledges the support of OTKA under grant T034764 (Hungary).

References and Notes

(1) Kohn, W.; Sham, L. J. *Phys. Rev. A* **1965**, *140*, 1133.

(2) Parr, R. G.; Yang, W. *Density Functional Theory of Atoms and Molecules*; Oxford University Press: Oxford, England, 1989.

(3) Redner, S. *Phys. Today* **2005**, *58*, 49.

(4) CAS Spotlight. http://www.cas.org/spotlight/bchem03/bchem03.html.

(5) Vosko, S. H.; Wilk, L.; Nusair, M. *Can. J. Phys.* **1980**, *58*, 1200.

(6) Perdew, J. P.; Wang, Y. *Phys. Rev. B* **1992**, *45*, 13244.

(7) Perdew, J. P.; Burke, K.; Ernzerhof, M. *Phys. Rev. Lett.* **1996**, *77*, 3865. Perdew, J. P.; Burke, K.; Ernzerhof, M. *Phys. Rev. Lett.* **1997**, *78*, 1396 (erratum). For other GGAs, see references therein.

(8) Tao, J.; Perdew, J. P.; Staroverov, V. N.; Scuseria, G. E. *Phys. Rev. Lett.* **2003**, *91*, 14 6401. For other meta GGAs, see references therein.

(9) Ernzerhof M.; Scuseria, G. E. *J. Chem. Phys.* **1999**, *110*, 5029.

(10) Becke, A. D. *Phys. Rev. A* **1988**, *38*, 3098.

(11) Lee, C.; Yang, W.; Parr, R. G. *Phys. Rev. B* **1988**, *37*, 785.

(12) Becke, A. D. *J. Chem. Phys.* **1993**, *98*, 5648.

(13) Stephens, P. J.; Devlin, F. J.; Chabalowski, C. F.; Frisch, M. J. *J. Phys. Chem.* **1994**, *98*, 11623.

(14) Perdew, J. P.; Ruzsinszky, A.; Tao, J.; Staroverov, V. N.; Scuseria, G. E.; Csonka, G. I. *J. Chem. Phys.* **2005**, *123*, 062201.

(15) Kurth, S.; Perdew, J. P.; Blaha, P. *Int. J. Quantum Chem.* **1999**, *75*, 889.

(16) Perdew, J. P.; Tao, J.; Staroverov, V. N.; Scuseria, G. E. *J. Chem. Phys.* **2004**, *120*, 6898.

(17) Staroverov, V. N.; Scuseria, G. E.; Tao, J.; Perdew, J. P. *J. Chem. Phys.* **2003**, *119*, 12129. Staroverov, V. N.; Scuseria, G. E.; Tao, J.; Perdew, J. P. *J. Chem. Phys*. **2004**, *121*, 11507 (erratum).

(18) Csonka, G. I.; Ruzsinszky, A.; Tao, J.; Perdew, J. P. *Int. J. Quantum Chem.* **2005**, *101*, 506.

(19) Staroverov, V. N.; Scuseria, G. E.; Tao, J.; Perdew, J. P. *Phys. Rev. B* **2004**, *69*, 075102.

(20) Perdew, J. P.; Kurth, S.; Zupan, A.; Blaha, P. *Phys. Rev. Lett.* **1999**, *82*, 2544. Perdew, J. P.; Kurth, S.; Zupan, A.; Blaha, P. *Phys. Rev. Lett.* **1999**, *82*, 5779. (erratum).

(21) Rabuck, A. D.; Scuseria, G. E. *Theor. Chem. Acc.* **2000**, *104*, 439.

(22) Staroverov, V. N.; Scuseria, G. E.; Perdew, J. P.; Tao, J.; Davidson, E. R. *Phys. Rev. A* **2004**, *70*, 012502.

(23) Tao, J.; Perdew, J. P. *J. Chem. Phys.* **2005**, *122*, 114102.

(24) Furche, F.; Perdew J. P. Unpublished work.

(25) Braida, B. Hiberty, P. C.; Savin, A. *J. Phys. Chem. A* **1998**, *102*, 7872.

(26) Grüning, M.; Gritsenko, O. V.; Gisbergen, S. J. A.; Baerends, E. J. *J. Phys. Chem. A* **2001**, *105*, 9211.

(27) Jaramillo, J.; Scuseria, G. E.; Ernzerhof, M. J. *Chem. Phys.* **2003**, *118*, 1068.

(28) Perdew, J. P.; Ernzerhof, M. In *Electronic Density Functional Theory: Recent Prospects and New Directions*; Dobson, J. F., Vignale, G., Das, M. P., Eds.; Plenum Publishing: New York, 1998.

(29) Gräfenstein, J.; Kraka, E.; Cremer, D. *J. Chem. Phys.* **2004**, *120*, 524.

(30) Becke, A. D. *J. Chem. Phys.* **2005**, *122*, 064101.

(31) Perdew, J. P.; Parr, R. G.; Levy, M.; Balduz, J. L. *Phys. Rev. Lett.* **1982**, *49*, 1961.

(32) Gunnarsson, O.; Lundqvist, B. I. *Phys. Rev. B* **1976**, *13*, 4279.

(33) Bauernschmitt, R.; Ahlrichs, R. *J. Chem. Phys.* **1996**, *104*, 9071.

(34) Perdew, J. P.; Savin, A.; Burke, K. *Phys. Rev. A* **1995**, *51*, 4531.

(35) Dunlap, B. I. *Adv. Chem. Phys.* **1987**, *69*, 287.

(36) Perdew, J. P.; Chevary, J. A.; Vosko, S. H.; Jackson, K. A.; Pederson, M. R.; Singh, D. J.; Fiolhais, C. *Phys. Rev. B* **1992**, *46*, 6671. Perdew, J. P.; Chevary, J. A.; Vosko, S. H.; Jackson, K. A.; Pederson, M. R.; Singh, D. J.; Fiolhais, C. *Phys. Rev.* **1993**, *48*, 4978 (erratum).

(37) Abrams, M. L.; Sherrill, C. D. *J. Chem. Phys.* **2004**, *121*, 9211.

(38) Zhao, Y.; González-Garcia, N.; Truhlar, D. G. *J. Phys. Chem. A* **2005**, *109*, 2012.

(39) Heyd, J.; Scuseria G. E. Unpublished work.

(40) Csonka, G. I.; Johnson, B. G. *Theor. Chem. Acc.* **1998**, *99*, 158.

(41) Kolos, W.; Wolniewicz, L. *J. Chem. Phys.* **1965**, *43*, 2429.

(42) Perdew, J. P.; Levy, M. *Phys. Rev. B* **1985**, *31*, 6269.

(43) Frisch, M. J.; Trucks, G. W.; Schlegel, H. B.; Scuseria, G. E.; Robb, M. A.; Cheeseman, J. R.; Montgomery, J. A., Jr.; Vreven, T.; Kudin, K. N.; Burant, J. C.; Millam, J. M.; Iyengar, S. S.; Tomasi, J.; Barone, V.; Mennucci, B.; Cossi, M.; Scalmani, G.; Rega, N.; Petersson, G. A.; Nakatsuji, H.; Hada, M.; Ehara, M.; Toyota, K.; Fukuda, R.; Hasegawa, J.; Ishida, M.; Nakajima, T.; Honda, Y.; Kitao, O.; Nakai, H.; Klene, M.; Li, X.; Knox, J. E.; Hratchian, H. P.; Cross, J. B.; Bakken, V.; Adamo, C.; Jaramillo, J.; Gomperts, R.; Stratmann, R. E.; Yazyev, O.; Austin, A. J.; Cammi, R.; Pomelli, C.; Ochterski, J. W.; Ayala, P. Y.; Morokuma, K.; Voth, G. A.; Salvador, P.; Dannenberg, J. J.; Zakrzewski, V. G.; Dapprich, S.; Daniels, A. D.; Strain, M. C.; Farkas, O.; Malick, D. K.; Rabuck, A. D.; Raghavachari, K.; Foresman, J. B.; Ortiz, J. V.; Cui, Q.; Baboul, A. G.; Clifford, S.; Cioslowski, J.; Stefanov, B. B.; Liu, G.; Liashenko, A.; Piskorz, P.; Komaromi, I.; Martin, R. L.; Fox, D. J.; Keith, T.; Al-Laham, M. A.; Peng, C. Y.; Nanayakkara, A.; Challacombe, M.; Gill, P. M. W.; Johnson, B.; Chen, W.; Wong, M. W.; Gonzalez, C.; Pople, J. A. *Gaussian 03*, revision C.01; Gaussian, Inc.: Wallingford, CT, 2004.

(44) Davidson, E. R.; Hagstrom, S. A.; Chakravorty, S. J.; Umar, V. M.; Froese-Fischer, C. *Phys. Rev. A* **1991**, *44*, 7071.

(45) Chakravorty, S. J.; Gwaltney, S. R.; Davidson, E. R.; Parpia, F. A.; Froese-Fischer, C. *Phys. Rev. A* **1993**, *47*, 3649.

(46) Perdew, J. P.; Zunger, A. *Phys. Rev. B* **1981**, *23*, 5048, and references therein.

(47) Zhang, Y.; Yang, W. *J. Chem. Phys.* **1998**, *109*, 2609.

(48) Mazziotti, D. A. *Phys. Rev. Lett.* **2004**, *93*, 213001.

(49) Krogh, J. W.; Olsen, J. *Chem. Phys. Lett.* **2001**, *344*, 578.

(50) Kinoshita, T.; Hino, O.; Bartlett, R. J. *J. Chem. Phys.* **2005**, *123*, 74106, and references therein.

(51) Polo, V.; Kraka, E.; Cremer, D. *Theor. Chem. Acc.* **2002**, *107*, 291.

(52) Andersson, K.; Roos, B. O. In *Modern Electronic Structure Theory*; Yarkony, D. R., Ed.; Advanced Series in Physical Chemistry; World Scientific: Singapore, 1995; Vol. 2, pp 55−109.

(53) Huber, K. P.; Herzberg, G. *Molecular Structure and Molecular Spectra IV: Constants of the Diatomic Molecules*; Van Nostrand Reinhold: New York, 1970.

(54) Clementi, E.; Chakravorty, S. J. *J. Chem. Phys.* **1990**, *93*, 2591. Savin, A.; Stoll, H.; Preuss, H. *Theor. Chim. Acta* **1986**, *70*, 407.

(55) Dietrich, D. L.; Anderson, J. *Science* **1992**, *258*, 786.

(56) Schultz, W. R.; Leroy, D. J. *J. Chem. Phys.* **1965**, *42*, 3869.

(57) Constantin, L.; Perdew, J. P.; Tao, J. Unpublished work.

(58) Kolos, W.; Wolniewicz, L. *J. Chem. Phys.* **1968**, *49*, 404.

(59) Perdew, J. P.; Levy, M.; Sagvolden, E. Unpublished work.

(60) Freire, H. J. P.; Egues, J. C. 0412491.

(61) Liu, J. W.; Hagstrom, S. *J. Phys. B: At. Mol. Opt. Phys.* **1994**, *27*, L729.

(62) Frye, D.; Lie, G. C.; Clementi, E. *J. Chem. Phys.* **1989**, *91*, 2366.